Liquid Crystals
Publication details, including instructions for authors and subscription information:
http://www.informaworld.com/smpp/title~content=t713926090

Photoinduced phase transitions

S. Krishna Prasad[a]; Geetha G. Nair[a]; D. S. Shankar Rao[a]
[a] Centre for Liquid Crystal Research, Jalahalli, Bangalore, India

To cite this Article Prasad, S. Krishna , Nair, Geetha G. and Rao, D. S. Shankar(2009) 'Photoinduced phase transitions', Liquid Crystals, 36: 6, 705 — 716
To link to this Article: DOI: 10.1080/02678290902755572
URL: http://dx.doi.org/10.1080/02678290902755572

Liquid Crystals,
Vol. 36, Nos. 6–7, June–July 2009, 705–716

Taylor & Francis
Taylor & Francis Group

INVITED ARTICLE

Photoinduced phase transitions

S. Krishna Prasad*, Geetha G. Nair and D. S. Shankar Rao

Centre for Liquid Crystal Research, Jalahalli, Bangalore 560 013, India

(Received 24 December 2008; final form 16 January 2009)

Employing actinic light to alter/stabilise a particular thermodynamic phase via the photo-isomerisation of the constituent molecules is an interesting tool to investigate soft matter from a new dimension. This article focuses on our recent results on several aspects of these non-equilibrium phase transitions, which are isothermal in nature. We specifically discuss (i) the influence of different parameters, such as confinement, applied electric field, pressure etc., on the dynamics associated with both the photochemical transition driving the equilibrium nematic to the non-equilibrium isotropic phase and the thermal back relaxation recovering the nematic phase, (ii) unique light-driven disorder–order transition in a reentrant system, (iii) dynamic self-assembly of the smectic A phase, which is stabilised only in the presence of actinic light, (iv) novel temperature-intensity phase diagrams and an example of primary and secondary photo-ferroelectric effects in an antiferroelectric smectic C system. These results highlight the fact that the actinic light can be used as a new tool to study phase transitions and the associated critical phenomena that could also bring about effects that are not seen in equilibrium situations.

Keywords: photoisomerisation; photoinduced transition; dynamic self-assembly; high pressure

1. Introduction

Molecules containing a chromophoric moiety such as azobenzene are well known to show reversible isomerisation transformations upon irradiation with UV and visible light (*1*). Upon absorption of UV light (~365nm) the energetically more stable E (also known as *trans*) conformation with an elongated rod-like molecular form transforms into a bent banana-like Z (or *cis*) conformation. The reverse transformation of the Z isomer into the E isomer can be brought about by irradiation of visible light (in the range of 400–500 nm). This latter change also occurs in the absence of any stimulation by a process known as *thermal back relaxation* (TBR). If the photoactive molecules are present in a system exhibiting liquid crystal phases then the isomerisation transformations mentioned above can lead to interesting influences on phase transitions. This is owing to the fact that the E form of the azobenzene, as it is rod-like, is favourable for the stabilisation of the liquid crystalline phase, whereas the Z form, which is in a bent shape, acts like an 'impurity' and therefore destabilises the liquid crystalline phase. The destabilisation can be significant enough even to cause an *isothermal* photoinduced transition from a liquid crystalline phase, say, the nematic phase to the isotropic phase. In fact, photoinduced effects have been well studied in systems exhibiting the nematic–isotropic (N–I) transition (*2*). In this article, we review some of our recent investigations on systems exhibiting the N–I transition, a reentrant nematic phase and a material having an antiferroelectric smectic phase.

2. Experimental

The molecular structures of the materials mentioned in this review are given in Figure 1. Although photo-isomerisation-related effects are large if the entire material is photoactive, from a practical point of view it is obviously better to dope small quantities of guest photoactive material into a host liquid crystalline system that exhibits the required phase sequence. For this purpose we have been employing guest–host systems, in which the host non-photoactive material is chosen with the kind of phase transition that is to be studied and the photoactive molecule as a guest compound. Unless otherwise mentioned the studies reviewed here have employed the compound EPH (see Figure 1 for the molecular structure) as the photoactive substance. The fact that the photoactive compound is also liquid crystalline helps in obtaining a homogeneous mixing of the guest and the host materials. The experimental setup employed for these studies is shown in Figure 2. The UV apparatus used for inducing photo-isomerisation consisted of an intensity stabilised UV source (peak wavelength: 365 nm) with a fibre-optic guide along with a UV-band pass filter. An additional IR-block filter was inserted just before the

*Corresponding author. Email: skpras@gmail.com

ISSN 0267-8292 print/ISSN 1366-5855 online

DOI: 10.1080/02678290902755572
http://www.informaworld.com

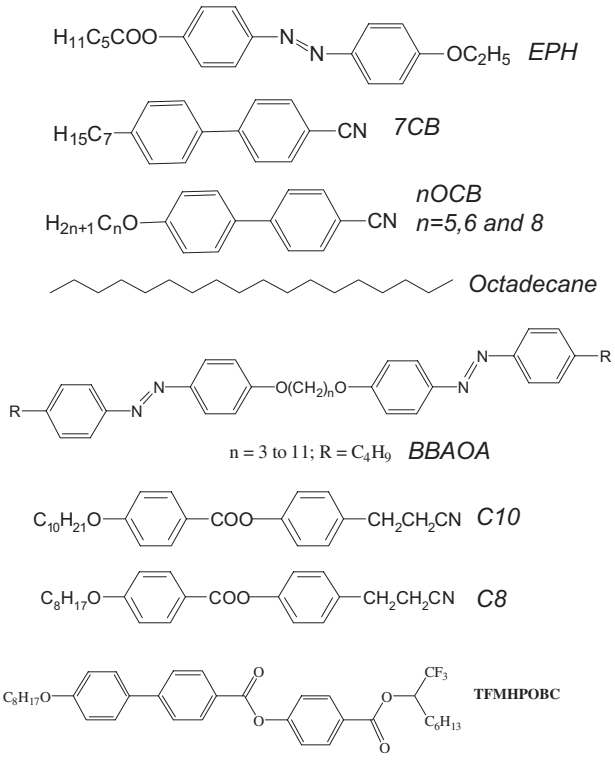

Figure 1. Chemical structures of the materials used for the experimental studies reviewed in this article.

sample to prevent any effects of heat radiation from the UV source. The actual power (I_{UV}) of the radiation passing through the filter combination and falling on the sample was measured with a UV power meter kept in the sample position.

3. Results and discussion

3.1 Nematic–isotropic transition

The nematic–isotropic transition is one of the simplest to be brought about by photoisomerisation of the photoactive molecules. The photo-driven isothermal phase transformation merely involves random rotation of the molecules, without any mechanical displacement. To begin with we look at the influence of confining the liquid crystal in an external matrix. The two scenarios considered are matrices formed from:

(1) A network generated by the dispersion of aerosil particles.
(2) Polymer dispersion.

3.1.1 Aerosil-LC

The liquid-crystalline material (which we refer to as LCM hereafter) used for these investigations is a 3.3% (by weight) mixture of the photoactive guest EPH in the non-photoactive host 7CB; the LCM mixture exhibits the N phase from 40.3°C down to sub-ambient temperatures. This material forms a gel when hydrophilic aerosil particles (diameter ~ 7 nm) are dispersed in it. The resulting gels are termed 'soft' or 'rigid' depending on a parameter called aerosil density (in g cm^{-3}), which is given by $\rho_a = m_a/V_{LC} = 0.03$, where m_a is the mass of aerosil and V_{LC} is the volume of LCM. Figure 3 shows the differential scanning calorimeter (DSC) scans obtained across the I–N transition for the pure LCM and a soft gel composite ($\rho_a = 0.03$) at different cooling rates. For the pure compound the scans contain a single peak at all scan

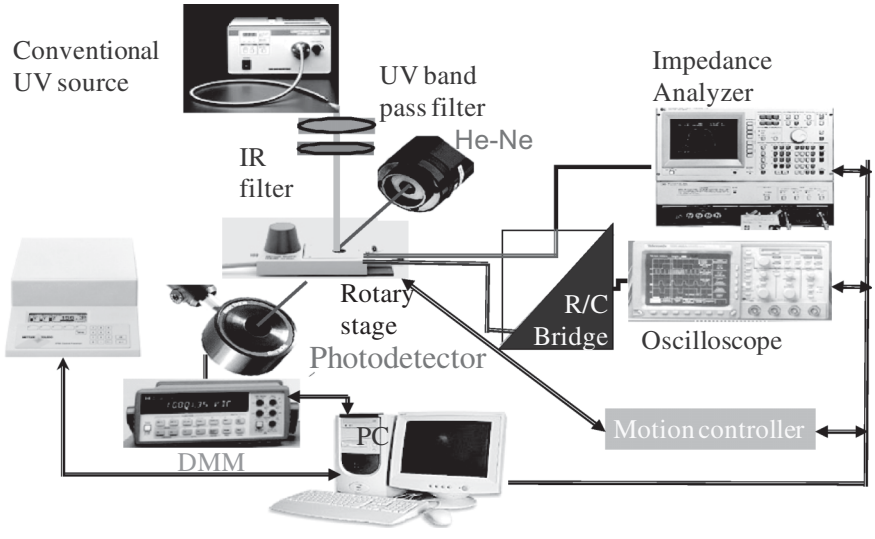

Figure 2. The schematic diagram of the experimental setup. For the high-pressure experiments the Mettler hot stage was replaced by the pressure cell described in (*16*).

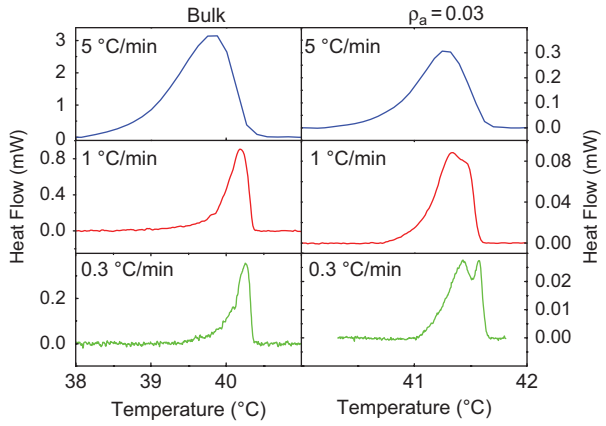

Figure 3. Left panels: differential scanning calorimetry (DSC) scans for the bulk (non-aerosil) sample obtained across the nematic–isotropic transition at three different cooling rates. Notice that there is only a single peak at all of the rates. Right panels: DSC scans for the $\rho_a = 0.03$ composite obtained across the nematic–isotropic transition for the same cooling rates as for the bulk. While for the fastest rate, 5°C min^{-1}, there is a single peak, clearly two peaks are seen for the lowest rate, 0.3°C min^{-1}. The profile obtained with the intermediate rate has a flattened top, suggesting that there may be two peaks.

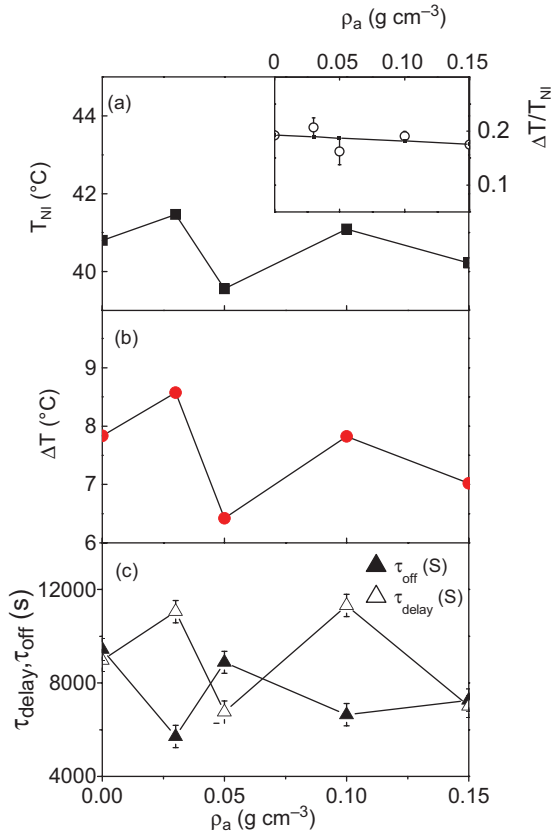

Figure 4. Influence of the aerosil composition on (a) the transition temperature T_{NI} and (b) the UV-induced shift in the transition temperature ΔT. The inset (in (a)) shows that the ratio of the two parameters is only weakly dependent on the aerosil concentration. The line drawn through the data points is a fit to a straight line and the error bars indicate 95% confidence limit. (c) Dependence of the τ_{delay} and τ_{off}, the delay in the initial response and the total time taken to complete the back relaxation respectively when the UV is switched off on the aerosil composition. Notice that the responses vary non-monotonically with the aerosil composition.

rates. In contrast, the aerosil mixture shows a rate-dependent behaviour. The point to be highlighted is the twin-peak profile seen for the composite at a cooling rate of 0.3°C min^{-1}. The observation of such a two-peak profile has been argued (*3*) to be owing to the development of nematic order from the isotropic phase through a two-step process in the case of the LC-aerosil systems. The two-step process arises (*4*) due to a crossover from a random-dilution regime, where the silica gel couples to the scalar part of the nematic order parameter, to a random-field regime (occurring at a lower temperature), in which the coupling induces distortions in the director field. It should also be noted that the high temperature peak is much sharper compared with the low temperature peak. This is to be expected since the high temperature region is associated with the appearance of the domains from the isotropic phase and with having a weak coupling to the aerosil network. The coupling becomes stronger in the region of the low-temperature peak and broadens it. The signature of the two-step process is prominently seen upon isomerisation of the photoactive component in the thermal and temporal variation of the dielectric constant of the sample, with the additional feature that the temperature difference between the two steps is increased in the UV-on situation. Another salient feature of these investigations is that not only T_{NI}, but ΔT, the photoinduced shift in T_{NI}, also varies non-monotonically with the aerosil density (see Figure 4(a) and (b)). However, the ratio of the two parameters is hardly dependent on the concentration (inset of Figure 4(a)). These results suggest that at least in the case of soft gels formed by the aerosil particles, the pinned-boundary-layer (PBL) model, according to which the LC molecules at the boundary layer are quenched and the remaining molecules behave as pure bulk material, is less favourable compared with the random field (RF) model in which the quenched LC is simply distributed randomly in space (*5*). Generally, the temporal decay of the capacitance after the UV is switched off can be described by a sigmoidal function, a feature characteristic of isothermal kinetics of phase transitions such as crystallisation (*6*). In the case of the $\rho_a = 0.03$ gel, the sigmoidal decay has an additional step, which is ascribed to the above-mentioned transformation

between the random dilution to the random field regimes. There were also indications that the dependence of the different time constants associated with TBR on ρ_a has a similar origin to that of T_{NI}: τ_{delay}, the delay time before the back relaxation begins, and varies in the same fashion as T_{NI}, but τ_{on}, the actual duration of the thermal back relaxation time, has the opposite behaviour (Figure 4(c)).

3.1.2 *Polymer matrix*

In this section we look at the effects of restricted geometry by confining the LC sample in a polymer matrix. This is achieved by UV-polymerisation of a photocurable prepolymer (Norland UV-curable optical adhesive NOA65) and a LC mixture (Merck-E7 + 5% EPH, referred to here as MON) in the ratio of 62/38; we refer to the polymerised sample as NOA. Figure 5 shows the TBR process for the MON and NOA samples (*7*). After the UV radiation is switched off, the MON sample responds slowly and exhibits a substantial time delay (~2000 s) between the time of switch-off and the instant at which there is an abrupt decrease in *C* (sample capacitance) marking the onset of the I–N transition. In contrast, the NOA sample responds instantaneously without any time delay. However, after the abrupt change further decrease of capacitance with time occurs at the same rate in both cases, as is shown in the inset by time-shifting the NOA data. This behaviour was found to be true for another polymer (polymethyl methacrylate) as well and explained by the

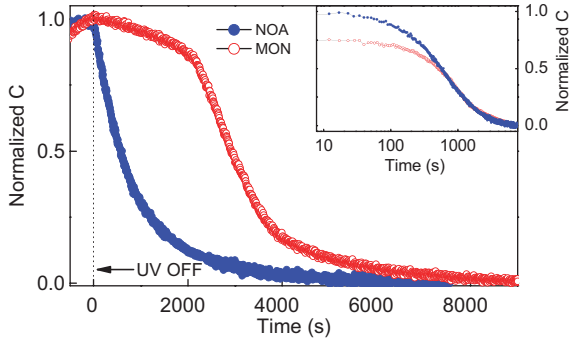

Figure 5. The thermal back relaxation processes for MON and NOA samples. After the UV is switched off, The MON sample responds slowly and exhibits a substantial time delay between the time at which the UV is switched off and the instant at which there is an abrupt decrease in C, marking the onset of the I–N transition. In contrast, the NOA sample, with the polymer matrix, responds instantaneously and has no time delay. However, once the abrupt decrease starts, the further decrease in time occurs at the same rate in both cases, as is shown in the inset. To illustrate this point, a time-shift is given to the NOA data, shown in the inset, to match the two sets at a value of 0.55 of the normalised C.

fact (*8*) that nematic order is known to persist at the surface even after the bulk has transformed into the isotropic phase. When UV is switched off this surface nematic order would promote the return of the photoinduced isotropic to the nematic phase in the bulk. In the case of the MON sample the surface order is present only at the two substrate surfaces, for the polymer-based samples the presence of the polymer matrix provides 'virtual surfaces', even in the bulk, at each liquid crystal–polymer interface, causing an acceleration of TBR and reduction of the delay time. Once the bulk starts recovering the N phase, the effect of the surface diminishes and therefore after the delay period the behaviour of the MON and NOA samples is quite similar.

3.1.3 *Influence of anisotropy-reducing component*

Now we discuss how the presence of a small concentration of a long chain normal alkane (octadecane, OD) can substantially increase the magnitude of TBR. OD and other such similar long chain alkanes have only flexible units and thus *per se* cannot and do not support the formation of liquid crystalline phases. Even when added to materials that already exhibit liquid crystalline phases they try to destabilise the liquid crystallinity (*9*); at the concentrations used in our experiments, the biphasic region is still small, suggesting that the structural incompatibility between the LC system and the alkane is still tolerable on a macroscopic scale. Owing to the preference of the alkane molecules to exist in the coil-form, there would be less difference between the local order in the vicinity of the alkane and the entire medium in the isotropic phase. On the other hand, in the nematic phase the alkane molecule is forced to deviate from the coil-form to be compatible with the environment. But given an opportunity to deviate from this situation, the alkane molecules may perhaps hinder the liquid crystalline molecules in the vicinity from achieving nematic order. For the temperature-dependent transition, such an influence will lower the transition temperature, a feature generally observed for liquid crystalline mixtures containing alkanes. In the case of photoinduced transition, the process is an isothermal one. Thus a possibility is that in the absence of any isomerisation-driven torques (e.g. presence of blue light to facilitate reverse isomerisation) the local disorder of the alkane molecules will retard the relaxation of the system from the photoinduced isotropic phase, thereby increasing the thermal back relaxation time τ_{off}. The magnitude of the effect increases, naturally, with increasing concentration of the alkane. Indeed, experiments show these arguments to be true (*10*) in the NLC mixture, having a photoactive component

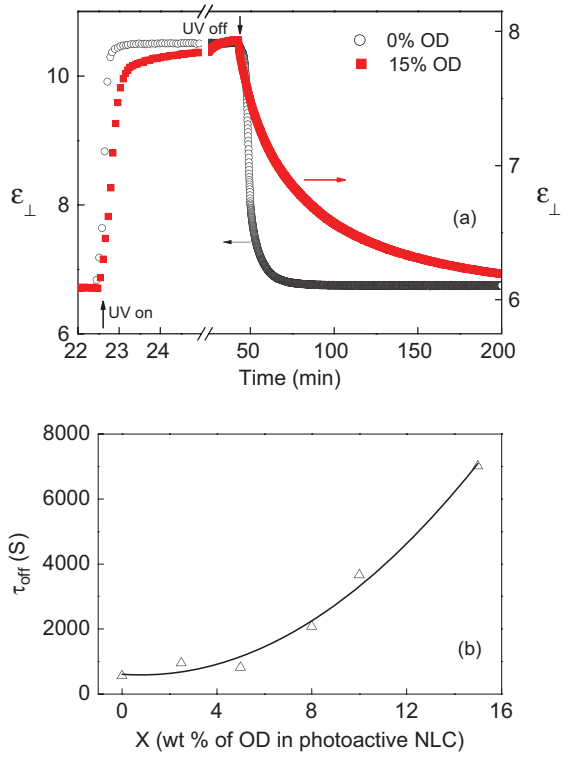

Figure 6. (a) UV On and UV Off dynamics for $X = 0$ (host material) and $X = 15$ mixture. Notice that the UV On dynamics takes about the same time for both materials, but the thermal back relaxation process takes much longer for the $X = 15$ mixture. (b) Dependence of the response times τ_{off} on the concentration of OD in the mixture. The line shown is only a guide to the eye.

and OD. While the duration of the photoinduced transformation is marginally increased, TBR shows a drastic increase (Figure 6(a)). In fact, TBR increases monotonically with concentration of OD becoming more than an order of magnitude higher for a concentration of 15% of OD (Figure 6(b)). Preliminary experiments also show that at a fixed reduced temperature, TBR increases by a factor of about 8 when the chain length of the alkane is increased from 16 to 24.

3.1.4 *Influence of the orientational order*

Detailed temperature dependent measurements (*11*) showed, surprisingly, that τ_{off} has a non-monotonic variation with temperature having a pronounced reduction (see Figure 7(a)) in the finite ΔT region bracketed by the two transition temperatures without ($T_{no\text{-}UV}$) and with UV ($T_{with\text{-}UV}$). The experiments also show that $\delta\varepsilon$, the difference in the dielectric anisotropy ε_a ($= \varepsilon_{||} - \varepsilon_\perp$) between the equilibrium and photostimulated situations, is finite only in the ΔT region (Figure 7(b)). We have used (*11*) this feature

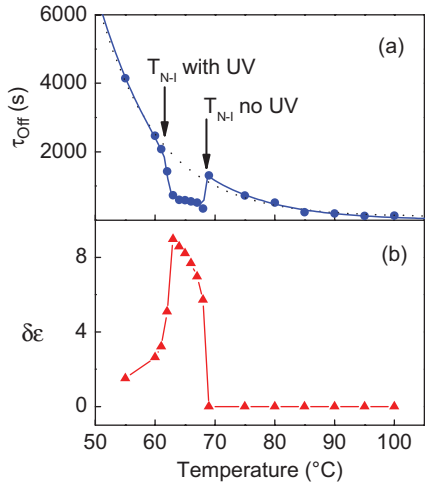

Figure 7. Thermal variation of the response time (a) τ_{off} and (b) $\delta\varepsilon$, the difference in the dielectric anisotropies for the no-UV and with-UV (1 mW cm^{-2}). The solid line in (a) is a fit to equation (1) and the dotted line represents Arrhenius behaviour.

and the proportionality of ε_a on the orientational order parameter of the N phase to explain the non-monotonic variation of τ_{off}. Adapting the Maier-Saupe model for the latter aspect, we have established a simple correlation between τ_{off} and $\delta\varepsilon$ as:

$$\tau_{off} = A + B\exp\left(\frac{-W}{k_B T}\right) - C\delta\varepsilon \qquad (1)$$

A least-square fitting of the data to Equation (1) is shown in Figure 7(a) as a solid line and is seen to describe the data well.

3.1.5 *Acceleration of TBR by an external field*

Figure 8(a) shows the fixed frequency dielectric constant data obtained for a planar sample in the absence of an electric field (except for the probing field) and when DC voltages of different magnitude are applied. It should be noted that since the material has a positive ε_a, application of a voltage V (above a Freedericksz threshold, which in this case is 2 V) reorients the molecules to be along the electric field direction; the extent of reorientation is controlled by the magnitude of the voltage, reaching saturation at higher values. Importantly, upon application of the electric field, the finite ΔT value realised by UV illumination is diminished (*12*). The temperature-voltage *phase diagram* (inset of Figure 8(a)) shows that the electric field opposes the formation/existence of the Z isomers, a behaviour confirmed by absorption measurements as well, and expresses itself in the time-resolved measurements also. Figure 8(b) shows the striking reduction of two orders of magnitude in τ_{delay} and a

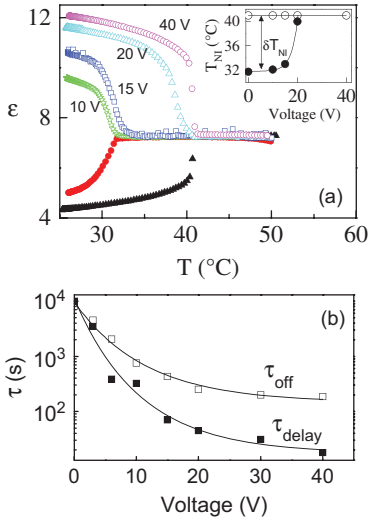

Figure 8. (a) Influence of the DC electric field on the photoinduced N–I transition. The voltages used are indicated against each curve. For comparison temperature dependence of the dielectric constant ε obtained with (filled circles) and without (filled triangle) the UV radiation is also plotted. Due to the positive dielectric anisotropy of the sample the application of the electric field reorientates the molecules from the surface determined planar to the high-field driven homeotropic orientation. As a consequence ε decreases across the N–I transition unlike in the field-off case. For the sake of convenience of presentation, the data in the isotropic phase has been matched between different sets. Inset: temperature–voltage phase diagram obtained without (○) and in the presence of (●) the UV radiation. Notice that there is no UV-induced diminution in the transition temperature for voltages greater than 20 V. The lines are only a guide to the eye. (b) Voltage dependence of the two time scales τ_{delay} (■) and τ_{off} (□) associated with the relaxation process (for definitions see text). The lines describe fit to an exponential function. Notice the nearly two orders of magnitude decrease in the timescales when the voltage applied is 40V.

factor of about 20 in τ_{off}, demonstrating that the application of the field does drastically accelerate the reverse isomerisation (*12*). This feature, seen for polar as well as non-polar LCs, is quite promising from the view point of E-Z photoisomerisation of photoactive molecules in general and in particular for the dynamic holograms and optical storage devices, and obviates the need for the radiation of a longer wavelength to achieve the recovery.

3.1.6 *Effect of elevated pressure*

The first ever high pressure study (*13*) of the effects of photoisomerisation on the N–I transition demonstrated that the application of pressure reduces the shift in the transition temperature induced by photoisomerisation, even leading to complete absence of such a shift above a certain pressure. A subsequent study (*14*), which also employed a monomeric photoactive molecule, confirmed this behaviour. From another point of view, investigations (*15*) had been carried out at atmospheric pressure on photoactive liquid crystalline dimer molecules. These measurements showed that the dimers acting as guest molecules in a host system substantially influence the static and kinetic characters of the photoinduced isothermal transition. For example, not only T_{NI} but ΔT, the photo-driven shift in the transition temperature, also exhibits an alternation with the parity of the spacer in the dimer molecule. With these features as background information, we performed high pressure investigations (*16*) on binary mixtures having 4-n-octyloxy cyano biphenyl (8OCB, for short) as the host material, and the C = 4 to 11 homologues of the series α,ω-Bis (4′-n-butylazobenzene-4-oxy) alkane (BBAOA), as the photoactive guest compounds; the mixtures are designated as M*n* (*n* = 4 to 11) where *n* indicates the number of methylene units in the spacer of the photoactive compound. Figure 9(a) and (b), shows the effect of applied pressure on the N–I phase boundary in the absence of and when UV illumination is done for the M4 and M5 mixtures. As expected, in both of the systems ΔT diminishes with increasing pressure and finally vanishes. However, P_o, the pressure at which the photoinduced boundary meets the equilibrium boundary, is substantially different for the two mixtures. Indeed its value alternates with the parity of the spacer in the guest molecule, but the direction of alternation is opposite to that of ΔT (see Figure 9(c)). Measurements at constant temperature have established that there is a decrease in the specific as well as transition volumes as the pressure and temperature are increased (*17*). Such a reduction in volume would mean that the intermolecular space available for the azobenzene molecule to take a bent shape decreases as the pressure is increased. In other words, the system opposes the formation of the Z isomers. Consequently, the photoinduced shift in the transition temperature caused by the Z isomer also becomes smaller as the pressure is increased and finally vanishes. It should be possible to counter, at least to a certain extent, this opposition due to reduction in the intermolecular space by increasing the energy of the UV radiation pumped into the system. This argument is found to be true experimentally, as the higher intensity level forces the E isomer of the azobenzene to transform to the Z isomer, leading to at least a partial restoration of the photoinduced shift in the transition temperature (*14*). The balance between these two opposing forces decides the pressure at which the shift becomes zero for a given intensity of the UV radiation. The applied pressure not only alters the phase boundary characteristics but also the dynamics associated with the photo-driven transition. For example, at a constant reduced

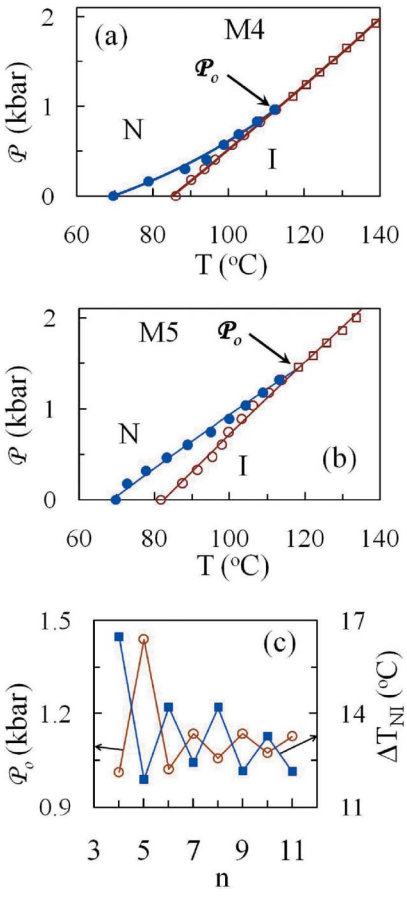

Figure 9. Pressure–temperature phase diagrams showing the nematic–isotropic phase boundary obtained when there is no UV radiation (open circles) as well as in the presence of 3.5 mW cm^{-2} UV radiation (filled circles), for the representative mixtures M4 (a) and M5 (b), respectively. The photoinduced shift in $T_{N\text{-}Iso}$ decreases with increasing pressure becoming zero at a pressure of $\mathcal{P}_o$. The solid lines are fit to the Simon–Glatzel equation. (c) Effect of the spacer length of the dopant dimeric molecule on ΔT (filled square), the photoinduced shift in $T_{N\text{-}Iso}$. Open circle represents odd–even behaviour of the pressure $\mathcal{P}_o$ at which the photoinduced shift in the transition ceases to exist as a function of the spacer length n. Notice that both the parity and the length of the spacer influence the value of not only ΔT but also the pressure $\mathcal{P}_o$.

temperature, τ_2, the response time for the photochemical change to occur, increases with increasing pressure whereas τ_3 and τ_4, the delay and response times for the back relaxation, decrease as pressure is increased (figure 10(a)). To be noted is the fact that increasing pressure at a constant temperature mimics the effects seen with decreasing temperature at a constant pressure; compare Figure 10(a) with 10(b). The features of this kinetics can also be explained using the argument of the fine balance between the opposing influences of the energy pumped and the pressure on the photoisomerisation. The odd–even effect caused by the parity of the spacer can be understood by considering the following:

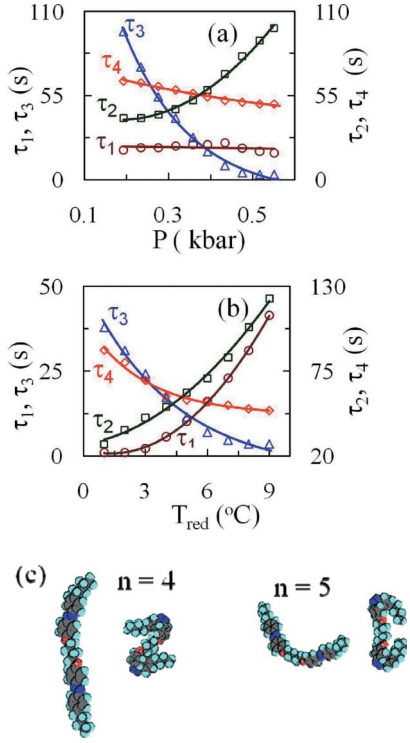

Figure 10. (a) Dependence of the delay (τ_1 and τ_3) and response times (τ_2 and τ_4) on the applied pressure at a constant reduced temperature of T_{red} = 5°C for the mixture M4. (b) Dependence of the delay (τ_1 and τ_3) and response times (τ_2 and τ_4) on the reduced temperature at a constant pressure of 0.55kbar for the mixture M4. (c) Minimum energy configurations in the E and Z conformer states for representative even (n = 4) and odd (n = 5) spacer dimer molecules.

(1) As expected, the E conformers of the even and odd spacers have, respectively, a somewhat elongated shape and a significantly bent shape (see Figure 10(c)).
(2) A remarkable change in the shape of the molecule, with the even member assuming a 'Z' shape and the odd member taking a 'C' shape upon isomerisation.
(3) The projected length l shows an alternation with m, the magnitude of the alternation being much larger for the E conformers than for the Z conformers. This larger change in the dimension of the even member molecules is the cause for the larger value of ΔT observed for them.

3.2 *Dynamic self-assembly of the smectic phase*

An important interplay between light and the structure of liquid crystals was first observed by Folks *et al.* (*18*) and has been excellently explained by simulation studies (*19*) invoking the concept of photo-driven nanophase segregation in smectic liquid crystals. This concept was extended by us to explain the experimental observation

of a photo-induced disorder-to-order transition (*20*), and induction of a layered mesophase in the presence of photo-irradiation (*21*, *22*); these observations are outlined below.

As a rule, a phase transition caused by the E–Z isomerisation of the constituent molecules always results in a reduction of the ordering of the medium, i.e. the transformation is an order-to-disorder transition. Another essential feature seen in photo-induced phase transitions is that the photo-induced phase would in any case occur in the thermal cycle. Exceptions to these features were found in the recent experimental results.

For these investigations a system exhibiting a reentrant nematic phase in the temperature-concentration phase diagram was chosen: specifically, for certain compositions, the system exhibits a nematic–smectic A–reentrant nematic (N–Sm-A–N_{re}) phase sequence when the sample was cooled from the isotropic phase. To be noted is the fact that the N phase exists both above and below the Sm-A phase, leading to the prefix, reentrant, for the lower temperature N phase owing to its reappearance on the temperature scale. When irradiated in the Sm-A and high temperature N phases, the material transforms into N and isotropic phases respectively, as expected, since the UV irradiation can lead to a 'melting' of the phase, or in other words, transformation to a less ordered state. But when the experiment was done in the N_{re} phase, a novel feature was observed (*20*): a transformation to the Sm-A phase, i.e. to a more ordered state (Figure 11).

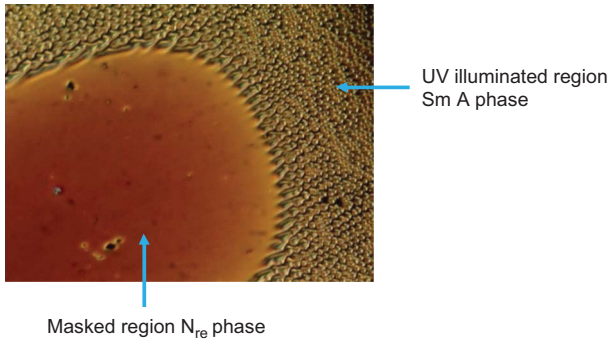

Figure 11. Optical polarising microscopy texture obtained for the $X = 60$ (wt% of C10 in C8 with 4% EPH) mixture in regions unexposed (N_{re} phase) and exposed (Sm-A phase) to UV radiation. (A hybrid geometry cell, in which the inner surface of one of the glass plates was coated with polyimide to get planar alignment, and that of the other with silane solution to promote homeotropic alignment of the molecules, was used.) The unexposed region showed the typical planar birefringent texture characteristic of the N phase, whereas the UV-exposed region transformed to focal conic texture, which is typical of the Sm-A phase. Also notable is the 'chevron' texture that appears at the interface between the masked and the UV illuminated regions.

A more exotic behaviour of dynamic self assembly of a simple orientationally ordered fluid phase into a layered phase only in the presence of UV light was observed in another photo-active system (*21*, *22*). In the absence of UV radiation the material did not exhibit the Sm-A phase. It was, however, induced and stabilised only in the presence of UV light. The smectic structure was self assembled with the UV radiation acting as a stimulant and existed only as long as the radiation was present.

These results can be explained in terms of the photo-controlled nanophase segregation mechanism (*19*) and the frustrated spin-gas model (*23*), the principles of which are outlined in the following. When the UV radiation is absent the azo molecules are in their E form, which has a rod-like shape and they are therefore easily accommodated into the smectic layers. In contrast, the photo-induced Z form of the molecule has a bent shape and owing its shape incompatibility is expelled from within the layers to a region between the layers. The dimension of the segregated regions is on the molecular scale, hence the label 'nanophase segregation'. The frustrated spin-gas model (*23*) is essentially designed for molecules that have a strong terminal polar group similar to the non-photoactive host used in our study. Frustration is built into the model by considering a triangular lattice of the molecules and their terminal dipole interactions leading to the stabilisation of the Sm-A or the N (N_{re}) phase, depending on the contribution of the dipole triplets to the free energy. Keeping these two features in mind, the following scenario can be imagined. Before photoisomerisation-driven segregation the molecules are free to librate along the director direction, thus stabilising the N (N_{re}) phase. On the other hand, the nanophase segregation due to photoisomerisation will create, in the segregated layers containing the photoactive Z molecules in their bent form, an alien atmosphere for the host rod-like molecules, thus disfavouring libration and as a consequence promote a layered arrangement, leading to the stabilisation of the Sm-A phase. X-ray and magnetic field driven Freedericksz transition experiments were carried out to confirm that the induced phase is indeed the Sm-A phase (Figure 12).

Novel temperature-UV intensity (T–I_{UV}) phase diagrams were also realised in the above mentioned system in which the UV intensity (of very low magnitudes ($I_{UV} < 100$ μW cm^{-2}), a non-thermodynamic quantity, acts as a variable (a representative diagram obtained for one composition is shown in (figure 13)). These studies, which showed that above a critical intensity, light induces and stabilises the Sm-A phase in mixtures not having that phase in the equilibrium situation (Figure 14), further demonstrated that light mimics, in a limited sense, the role of a thermodynamic

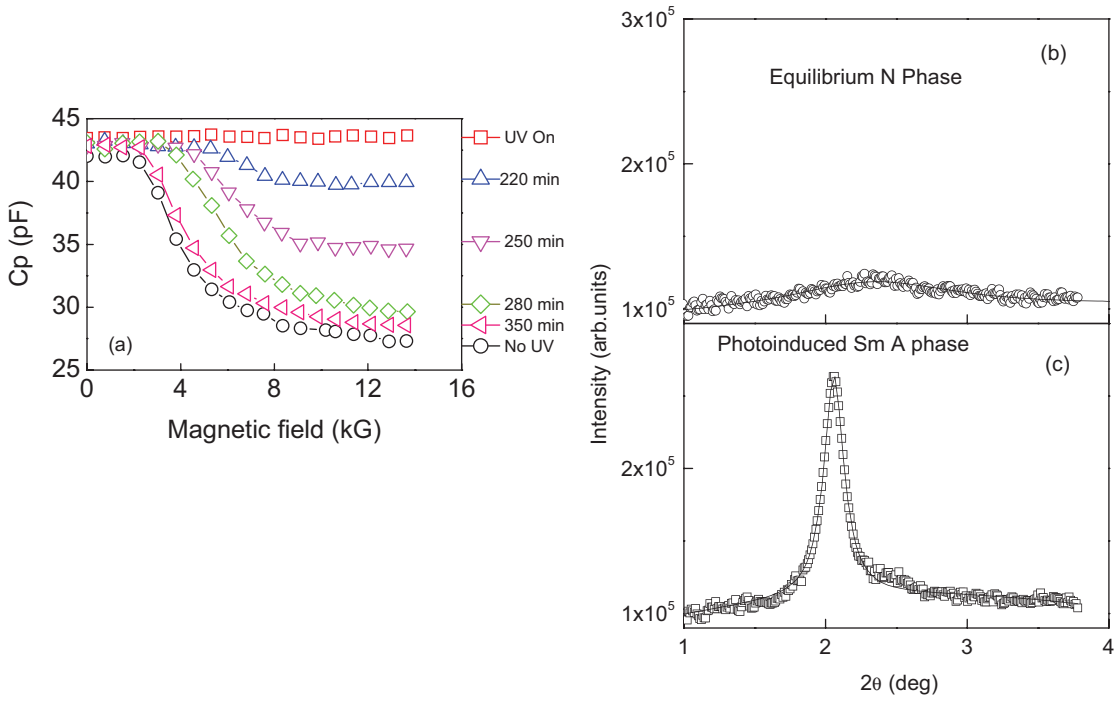

Figure 12. (a) Magnetic-field driven Freedericksz transition studies for $X = 60$. The data obtained at $T = 38^{o}$C in the absence of (open circles) and upon illumination with (open squares) UV radiation. The non-existence of the Freedericksz transition for the latter set supports the microscopic observations (shown in Figure 11) of a photo-stabilised Sm-A phase. The sets of data obtained at time instants ranging from 220 to 350 minutes after the UV light was switched off when the system was undergoing thermal back relaxation and recovering the N phase are also shown. X-ray diffraction patterns obtained in (b) the equilibrium N phase and (c) the photoinduced Sm-A phase. Notice the profile becomes quite sharp and intense in the Sm-A phase.

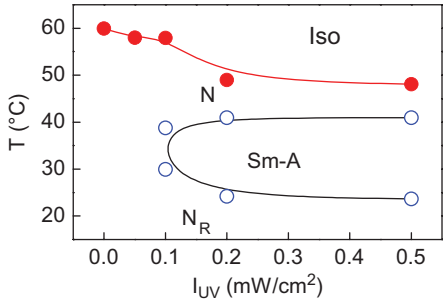

Figure 13. T–I_{UV} phase diagrams for $X = 55$ (wt% of C10 in C8 with 4% EPH).

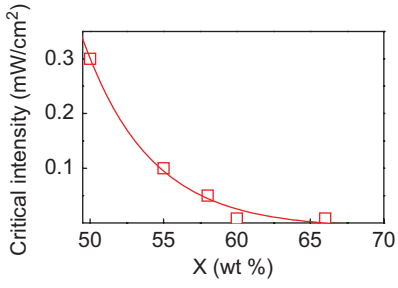

Figure 14. Concentration (X) dependence of the critical intensity (I_c) required to induce the Sm-A phase. The critical intensity I_c diverges as the concentration moves away from the tip of the parabola in the T–X diagram (*21*).

parameter like, for example, pressure (*24*). These studies also suggest the possibility of observing a double critical point (DCP), which by definition is the meeting point of two critical lines (N–Sm-A and Sm-A–N_{re} boundaries). The advantage of UV intensity as a control parameter for such a purpose over that of concentration or pressure is the ease with which the magnitude of the intensity can be controlled. It should, however, be pointed out that:

(1) The UV intensity is not an actual thermodynamic parameter and therefore the features seen in the T–I_{UV} plane may be different from those in the T–X plane.

(2) T–I_{UV} phase diagrams are non-equilibrium situations unlike those in the T–X or T–pressure planes.

3.3 Polarisation-tilt coupling in an antiferroelectric system

A variant of the Sm-C* phase was reported in 1989 in which the molecules in neighbouring layers are tilted from the smectic layer normal in almost opposite directions (*25*). This phase is called the antiferroelectric Sm-C* or Sm-C_A^* phase. We recently (*26*) performed a detailed study of the effect of photoisomerisation on the temperature variation of electric polarisation, tilt angle and dielectric properties in a system exhibiting the Sm-A–Sm-C_A^* transition. The material used for these studies is a binary mixture referred to as AF mixture composed of TFMHPOBC exhibiting Sm-A–Sm-C_A^* transition as the host and 5% by weight of the guest UV-active dopant EPH.

In the antiferroelectric Sm-C_A^* phase, application of triangular and sinusoidal wave fields to the sample yielded, respectively, a two-peak trace per half cycle of the applied field and a double hysteresis loop, features that are characteristics of the tri-state switching expected for the phase. The temperature dependence of the electric polarisation (P_s) determined from the combined area under the two-peak trace in the absence of the UV radiation and upon illuminating the sample with the magnitude of UV intensity I_{UV} = 4 mW cm^{-2} is shown in Figure 15. Although the gross trend remains the same with and without UV, two distinguishing features seen in the presence of UV radiation are that there is a reduction in T_c (the Sm-A–SmC_A^* transition temperature) and that the saturated value of P_s achieved deep in the Sm-C_A^* phase is substantially lower than that without UV illumination. We refer to the first feature commonly seen in the area of photoinduced phase transitions and also discussed above, as the *secondary photoferroelectric effect* (*27*). The reduction of ~30% in P_s found even after accounting for the reduction in T_c should be associated with a change in the polar ordering and/or the transverse molecular dipole moment and is labelled primary photoelectric effect (PPE). To look at this effect from a quantitative point of view, we considered various possibilities. In ferroelectric as well as antiferroelectric LC systems the tilt angle of the molecules (θ) with respect to the layer normal is the primary order parameter and the electric polarisation P_s is a secondary order parameter. As P_s is strongly coupled to θ, a trivial cause for the observed PPE could be the primary photoclinic (light-driven tilt of the molecules) effect. However, tilt angle measurements carried out with and without UV illumination show that there is only a secondary effect, which can be accounted for by a shift in T_c.

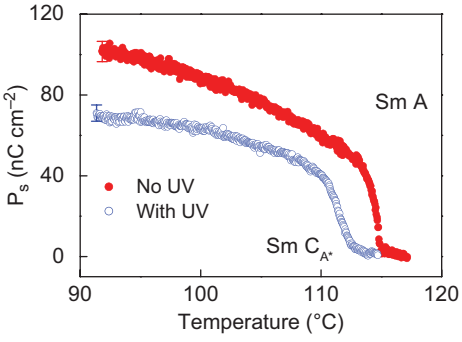

Figure 15. Temperature dependence of the spontaneous polarisation (P_s) in the absence of UV (top curve) and when the sample is illuminated with I_{UV} = 4 mW cm^{-2} (bottom curve). Notice the reduction in the P_s value as well as a shift in the transition temperature for the UV-illuminated case. A reduction of ~30% in P_s was found even after accounting for the reduction in T_c.

The second possibility that we looked at is the nanophase segregation mechanism, which is suitable particularly for layered smectic phases. The essence of this mechanism has already been given in Section 3.2. When such a segregation takes place, the bend directions of the EPH molecule in the segregated layer can be random . Further, owing to the increase in the layer thickness upon segregation there would be an apparent increase in the volume of the system with a consequential reduction in the dipole moment and/or volume. Hence the measured P_s would be lower than before UV illumination. However, the maximum observed increase in layer spacing upon UV illumination is quite small (~0.05 nm) with a resulting change in volume of ~1%. The associated decrease in dipole moment/unit volume and thus of P_s should be of the same order, but the measured P_s decrease is much larger (30%).

Therefore, we look at the possibility of the photoisomerisation altering the coupling between P_s and θ in a quantitative fashion. The behaviour of P_s and θ, mentioned above, suggests that the P_s/θ ratio decreases upon UV illumination. The generalised mean field model (*28*) that incorporated a 6th order term in θ to account for the possibility of first order transition and a biquadratic coupling term $-P_s^2\theta^2/2$ to bring in transverse quadrupolar ordering (which is non-chiral in character) has been quite successful in getting realistic explanations of the P_s-θ coupling. In the absence of certain terms that were introduced purely for stability reasons or terms containing the helical pitch (which would be unwound in the present experiments), the model is written as:

$$F = Fo + \frac{a}{2}\theta^2 + \frac{b}{4}\theta^4 + \frac{c}{6}\theta^6 + \frac{P_s^2}{2\chi} - CP_s\theta - \frac{\Omega}{2}P_s^2\theta^2 - P_sE \qquad (2)$$

and yields a simple relation between P_s and θ:

$$P_s = \frac{C\theta}{1/\chi - \Omega\theta^2} \qquad (3)$$

In this model an all important parameter $\beta \infty C/\Omega$ was considered, whose value governs the temperature dependence of the P_s/θ ratio.

The P_s vs. θ data in the absence and upon UV illumination are given in Figure 16, along with the fitting done using Equation (3). The striking feature to be noted is that while the no-UV data has a significant curvature, the data obtained under UV illumination is highly linear (in fact, a fit done to the expression for a straight line yields only a slightly lower quality fit). The coefficients C and were found to be $4.4 \pm 0.1 \times 10^7$ V m^{-1}, $8.2 \pm 0.4 \times 10^{10}$ Nm^{2}C^{-2} for the no-UV data set and $5.2 \pm 0.2 \times 10^7$ V m^{-1}, $1.8 \pm 0.1 \times 10^{10}$ N m^2 C^{-2} for the data with UV illumination. These values are of the same order of magnitude as for other ferroelectric liquid crystals (*28*). Note that while the chiral coefficient C increases slightly (~17%) upon UV illumination, the non-chiral coefficient shows a large change, decreasing by a factor of 4. In other words, UV illumination reduces the non-chiral aspect of the P_s-θ coupling, thus supporting the qualitative change in the behaviour of the P_s vs. θ data from non-linear trend to a linear one as shown in

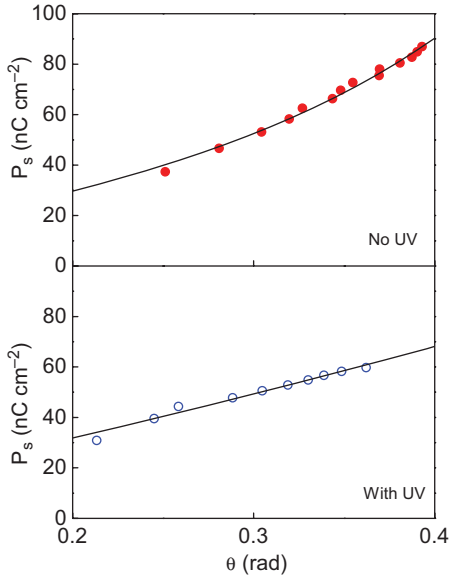

Figure 16. Tilt angle dependence of polarisation in the absence of (top panel) and upon shining UV (bottom panel). Notice that the no-UV data has a significant curvature, whereas the data obtained with UV (I_{UV} = 4 mW cm^{-2}) is nearly linear. The fit to Equation (3) (shown as solid lines) describes the data well in both cases.

Figure 16. The C/Ω ratio, which governs the temperature dependence of the P_s/θ ratio, increases by a factor of 5 upon UV illumination. For comparison with the theoretical predictions, we consider the ratio of C/Ω suitably normalised as the parameter β' and the model parameter β, which has a value between 0 and 1. For the no-UV and with-UV cases, β' increases from 0.2 to 0.5. According to the theory such a large variation means that there should be a substantial change in the thermal behaviour of the P_s/θ ratio, a feature seen to be true (Figure 17) in the experiments: for the no-UV case the ratio varies over the entire temperature range of measurement, but the data collected with UV remains essentially constant except in the vicinity of the transition. This analysis is further supported by the UV-intensity dependence of the thermal variation of the strength (*29*) of the dielectric soft mode relaxation (Figure 18(a)), which can again be explained on the basis of the increase in β' with UV illumination, and is in qualitative agreement

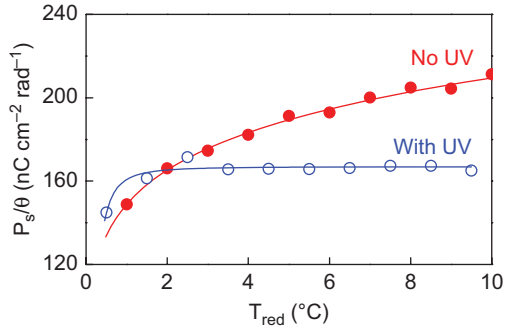

Figure 17. The dependence of the P_s/θ ratio on the reduced temperature T_{red} for the no-UV and with-UV (I_{UV} = 4 mW cm^{-2}) conditions. The former has a variation with temperature throughout the range shown, whereas under UV illumination the ratio is nearly constant except near the transition (T_{red} = 0). The solid lines are a guide to the eye only.

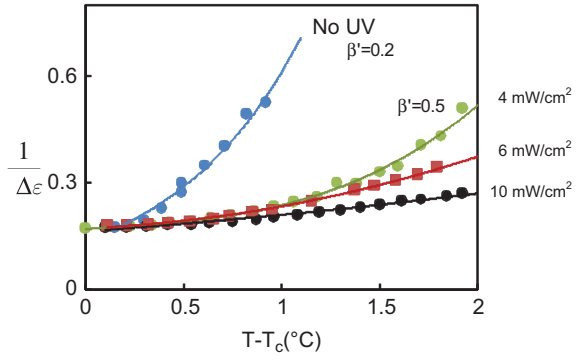

Figure 18. The influence of the magnitude of I_{UV} on the thermal variation of the soft mode dielectric strength. The β' values were evaluated using the P_s and θ data (see text).

(Figure 18(b)) with the predictions of the Landau model (*30*). A possible molecular level argument for these observations is on the lines of the guest–host effect of P_s in induced Sm-C* phases (*31*). Mutual steric interactions, and consequent mutual orientation directions of the steric dipoles of the guest photoactive molecules and the host non-photoactive molecules play an important role here.

Acknowledgements

We sincerely appreciate the participation of the students of our Centre Dr. Gurumurthy Hegde, Ms. V. Jayalakshmi, Drs. Chethan Vishal Lobo, K.L. Sandhya and Dr. Vivek Kumar Gupta, P.G. Department of Physics, University of Jammu, Jammu in this programme. Thanks are also due to our colleagues Dr. C.V. Yelamaggad and Dr. Uma S. Hiremath and Dr. Negi (then at Centre for Materials for Electronics Technology, Panchwati, Pune) for providing some of the samples used in these studies. Partial financial support by SERC, DST, New Delhi under a project is gratefully acknowledged.

References

(1) See, e.g. Rau, H., Photoisomerization of Azobenzenes. In *Photochemistry and Photophysics*, Rabeck, F.J., Ed.; CRC, Boca Raton, FL, 1990; Vol. 2, Chap. 4.
(2) For earlier reviews, see Prasad, S.K.; Nair, G.G.; Hegde, G.; Sandhya, K.L.; Rao, D.S.S.; Lobo, C.V.; Yelamaggad, C.V. *Phase Transitions* **2005**, *78*, 443–455; Ikeda, T., *J. Mater. Chem*. **2003**, *13*, 2037–2057; Prasad, S.K.; Nair, G.G.; Sandhya, K.L.; Rao, D.S.S. *Curr. Sci.* **2004,** *86*, 815–823.
(3) Jayalakshmi, V.; Nair, G.G.; Prasad, S.K. *J. Phys.: Condens. Matter* **2007**, *19*, 226213-1-12.
(4) Caggioni, M.; Roshi, A.; Barjami, S.; Mantegazza, F.; Iannacchione, G.S.; Bellini. T. *Phys. Rev. Lett*, **2004**, *97*, 127801-1-4.
(5) For a summary of the theoretical models, see Iannacchione, G.S. *Fluid Phase Equilibria*. **2004**, *222–223,* 177–187; Lobo, C.V.; Prasad, S.K.; Yelamaggad, C.V. *J. Phys.: Condens. Matter* **2006,** *18*, 767–776.
(6) See e.g. Hu, Y.S.; Rogunova, M.; Schiraldi, D.A; Hiltner, A.; Baer, E. *J. Appl. Polym. Sci* **2002**, *86*, 98–115.
(7) Sandhya, K.L.; Prasad, S.K.; Nair, G.G.; Hegde, G. *Appl. Phys. Lett*. **2003**, *83*, 2707–2709.
(8) Miyano, K. *Phys. Rev. Lett.* **1979**, *43*, 51–54; Sheng, P. *Phys. Rev. A.* **1982,** *26*, 1610–1617.
(9) Orendi, H.; Ballauff, M. *Liquid Crystals* **1989**, *6*, 497–500.
(10) Nair, G.G.; Prasad, S.K.; Hegde, G. *Phys. Rev. E* **2007**, *69*, 021708-1-6.
(11) Jayalakshmi, V.; Nair, G.G.; Prasad, S.K. *Phys. Rev. E* **2007**, *75*, 031710-1-6.
(12) Prasad, S.K.; Nair, G.G.; Jayalakshmi, V. *Adv. Mater.* **2008**, *20*, 1363–1367.
(13) Prasad, S.K.; Rao, D.S.S.; Jeyagopal, P. *Phys. Rev. E* **2001**, *64*, 011706-1-4.
(14) Prasad, S.K.; Gupta, V.K.; Rao, D.S.S.; Lobo, C.V. *Phys. Rev. E* **2005**, *72*, 021705-1-6.
(15) Prasad, S.K.; Sandhya, K.L.; Nair, G.G.; Yelamaggad, C.V.; Hiremath, U.S. *J. Appl. Phys.* **2002**, *92*, 838–841.
(16) Gupta, V.K.; Rao, D.S.S.; Lobo, C.V.; Prasad, S.K.; Yelamaggad, C.V.; Hiremath, U.S. *Thermochimica Acta* **2006**, *440*, 205–211.
(17) Transfeld, R.V.; Collings, P.J. *Phys. Rev. A* **1982**, *25*, 2744–2749.
(18) Folks, W.R.; Keast, S.; Krentzel, T.A.; Zalar, B.; Zeng, B.H.; Reznikov, Yu. A.; Neubert, M.; Kumar, S.; Finotello, D.; Lavrentovich, O.D. *Mol. Cryst. Liq. Cryst.* **1998**, *320*, 77–88.
(19) Lansac, Y.; Glaser, M.A.; Clark, N.A.; Lavrentovich, O.D. *Nature* **1999**, *398*, 54–57.
(20) Prasad, S.K.; Nair, G.G. *Adv. Mater*. **2001**, *13*, 40–43.
(21) Prasad, S.K.; Nair, G.G.; Hegde, G. *Adv. Mater*. **2005**, *17*, 2086–2091.
(22) Prasad, S.K.; Nair, G.G.; Hegde, G. *J. Phys. Chem. B* **2007**, *111*, 345–350.
(23) Berker, A.N.; Walker, J.S. *Phys. Rev. Lett.* **1981**, *47*, 1469–1472.
(24) Kalkura, A.N.; Shashidhar, R.; Subramanya Raj Urs, M. *J. Physique* **1983**, *44*, 51–55.
(25) Chandani, A.D.L.; Gorecka, E.; Ouchi, Y.; Takezoe, H.; Fukuda, A. *Jpn. J. Appl. Phys. Part 2* **1989**, *28*, L1265–1268.
(26) Nair, G.G.; Hegde, G.; Prasad, S.K.; Lobo, C.V.; Negi. Y.S. *Phys. Rev. E* **2006**, *73*, 011712-1-9.
(27) Langhoff, A.; Giesselmann, F. *Chem. Phys. Chem*. **2002**, *3*, 424–432.
(28) Carlsson, T.; Zeks, B.; Filipic, C.; Levstik, A.; Blinc, R. *Mol. Cryst. Liq. Cryst.* **1988**, *163*, 11–72.
(29) Nair, G.G.; Hegde, G.; Prasad, S.K.; Negi, Y.S. *J. Phys.: Condens. Matter* **2006**, *18*, 9415–9425.
(30) Carlsson, T.; Zeks, B.; Filipic, C.; Levstik, A. *Phys. Rev. A* **1990**, *42*, 877–889.
(31) Stegemeyer, H.; Meister, R.; Hoffmann, U.; Sprick, A.; Becker, A. *J. Mater. Chem*. **1995**, *5*, 2183–2193.